Probabilistic Earthquake Relocation in Three-Dimensional Velocity Models for the Yellowstone National Park Region, Wyoming

by Stephan Husen* and Robert B. Smith

Abstract Recorded seismicity for the Yellowstone National Park region, comprising 25,267 earthquakes from November 1972 to December 2002, has been relocated using three-dimensional velocity models and probabilistic earthquake location. In addition, new coda magnitudes for earthquakes between 1984 and 2002 were computed by using an improved coda magnitude equation. Three-dimensional velocity models for earthquake location were computed by inverting subsets of high-quality data of three different periods, 1973–1981, 1984–1994, and 1995–2002, for hypocenter locations and seismic velocities. Earthquakes were relocated by using a nonlinear, probabilistic solution to the earthquake location problem. Fully nonlinear location uncertainties included in the probabilistic solution allow a better and more reliable classification of earthquake locations into four quality classes. Earthquake locations show an improvement in location accuracy with time, which we attribute to improved network geometry and more precise timing of arrival times. No large systematic shifts of the relocated earthquake locations are observed, except a systematic shift of ~2 km to greater depth. The new relocated earthquake locations show tighter clustering of epicenters and focal depths when compared with original earthquake locations. The most intense seismicity in terms of number of earthquakes and cumulative seismic moment release in the Yellowstone National Park region occurs northwest of the Yellowstone caldera between Hebgen Lake and the northern rim of the caldera. Seismicity within the Yellowstone caldera is diffuse, and shallow individual clusters of earthquakes can be associated with major hydrothermal areas.

Introduction

With more than 20,000 earthquakes since 1973, the Yellowstone National Park region, Wyoming, hereafter called Yellowstone, is the most seismically active area of the 1,300-km-long Intermountain Seismic Belt (ISB), which extends from northern Montana to northern Arizona (Smith and Arabasz, 1991). In general, seismicity in Yellowstone (Fig. 1) is the result of the interaction of the Yellowstone volcanic system with an extending lithosphere of the Basin and Range province. Yellowstone is centered on the 10,000-km^2 volcanic Yellowstone plateau, which was formed by three major caldera-forming eruptions during the past two million years. The youngest eruption at 0.64 mega annum (Ma) (Christiansen, 2001) created the current Yellowstone caldera (Fig. 1). After the formation of the Yellowstone caldera, at least 30 rhyolite flows as young as 70,000 years covered the Yellowstone area (Christiansen, 2001), thereby covering older Basin and Range normal faults.

Yellowstone's youthful volcanic history is the main source of heat driving the expansive hydrothermal system (Fournier and Pitt, 1985), which is manifest on the surface by more than 10,000 geysers, hot springs, and fumaroles. Localized transport of magma and hydrothermal fluid within the Yellowstone caldera and the influence of the regional stress field of the Basin and Range province form the background for the high seismicity in Yellowstone, including the 1959 *M* 7.5 Hebgen Lake, Montana, earthquake, the largest historic normal faulting earthquake in the Intermountain Seismic Belt (Smith and Arabasz, 1991).

Since 1973, seismicity in Yellowstone has been routinely monitored by permanent seismic networks. Changes in network design and the use of linearized earthquake location techniques in combination with one-dimensional velocity models, however, limit the consistency and detailed use of the earthquake locations in Yellowstone. Studies of seismotectonics and seismic hazard, for example, rely critically on the accuracy of earthquake locations. Location uncertainties derived from linearized earthquake location are based on a linear approximation to a set of nonlinear equations and can be inaccurate and unreliable (Lomax *et al.*,

---

*Present address: Swiss Seismological Service, ETH Hoenggerberg, CH 8093 Zurich.
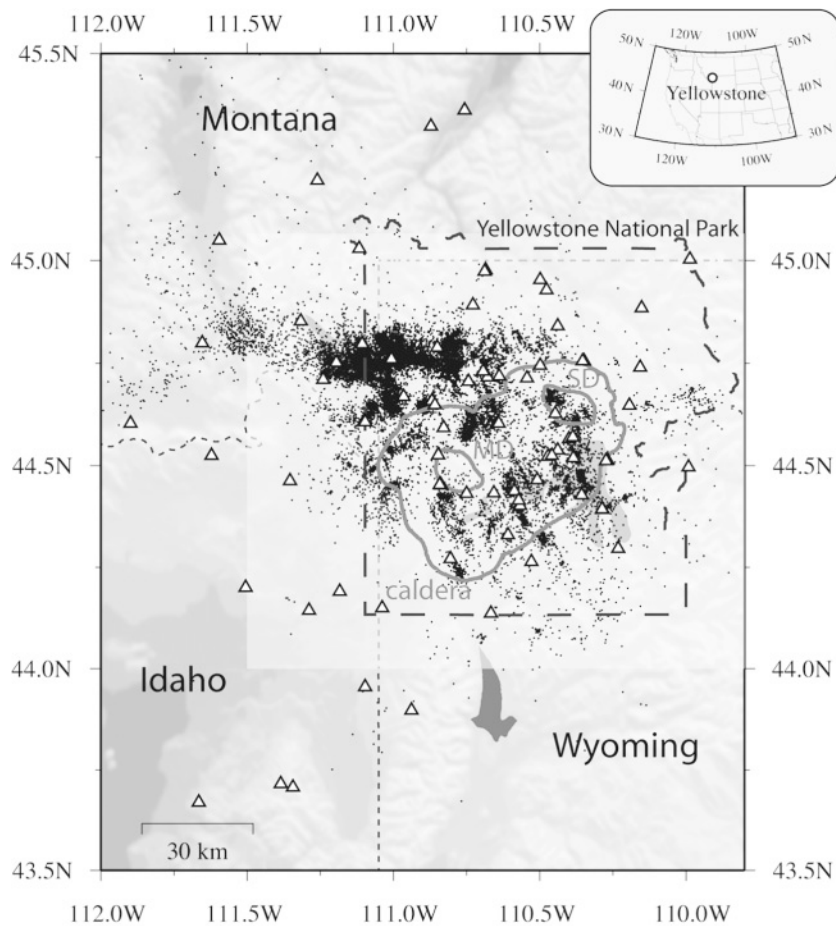
Figure 1. Map of the greater Yellowstone National Park region. Routine earthquake locations from 1973 to 2002 are shown by black dots. Seismic stations operating between 1973 and 2002 are shown by white triangles; note that not all stations were operating simultaneously. The 0.64 Ma Yellowstone caldera and the two resurgent domes inside the caldera are outlined by gray lines; MD, Mallard resurgent dome, SD, Sour Creek resurgent dome. Heavy dashed line marks boundary of the Yellowstone National Park; thin dashed line marks state boundaries. Light-colored box denotes Yellowstone National Park region, for which a relocated earthquake catalog is presented in this study.

2000; Husen *et al.*, 2003a). Moreover, one-dimensional velocity models are a poor approximation to Yellowstone's crustal structure affected by active volcanism.

Earthquake locations between 1973 and 1994 were routinely published in various reports (Smith, 1985, 1986; Pitt, 1987; Smith and Nagy, 1987; Nagy and Smith, 1989b; Peyton and Smith, 1990; Nava and Smith, 1993, 1996). The first comprehensive study of seismicity between 1973 and 1989 in Yellowstone was done by Smith and Arabasz (1991). They used earthquakes of magnitude greater than two routinely located by the U.S. Geological Survey (1973–1981) and by the University of Utah Seismograph System (1984–1989). A major outcome of this study was a decrease of focal depths beneath the Yellowstone caldera. Earthquakes located outside the Yellowstone caldera showed maximum focal depths of up to 15 km, whereas maximum focal depths beneath the Yellowstone caldera were less than 5 km. This pattern of shallowing in focal depth suggested a thin layer of seismogenic brittle upper crust beneath the Yellowstone caldera (Smith and Arabasz, 1991). Miller and Smith (1999) relocated 7942 earthquakes between 1973 and 1994 as part of their local earthquake tomography study in Yellowstone. Hypocenter locations of these earthquakes were obtained by linearized earthquake location in a three-dimensional velocity model. The most visible effect of their relocation study

was a better clustering of earthquakes in the southwestern and eastern central Yellowstone caldera. Focal depths of these relocated earthquakes showed a similar shallowing beneath the Yellowstone caldera as previously observed by Smith and Arabasz (1991).

Increasing computing power and recent developments in earthquake location techniques now allow the use of nonlinear, probabilistic earthquake location with any available velocity model. The combination of nonlinear, global search algorithms, such as the Oct-Tree Importance Sampling (Lomax and Curtis, 2001), with probabilistic earthquake location provides a fast and reliable tool for earthquake location (Husen *et al.*, 2003a). Among the benefits of using three-dimensional velocity models, probabilistic earthquake location provides a complete description of location uncertainties (Lomax *et al.*, 2000). Because the solution is fully nonlinear, location uncertainties may be irregular and multimodal, hence departing from the traditional description by error ellipsoids.

In this study, we relocated seismicity recorded in Yellowstone, encompassing 25,267 earthquakes from November 1972 to December 2002, using three-dimensional velocity models and probabilistic earthquake location. In addition, we recomputed coda magnitudes for 19,097 earthquakes from January 1984 to December 2002, using newly available

instrument calibrations and an improved coda magnitude equation. Three-dimensional velocity models were obtained by local earthquake tomography for three different periods, 1973–1981, 1984–1994, and 1995–2002, using a subset of high-quality earthquake data for each period. Because examination of the fully nonlinear location uncertainties for each earthquake location is not practicable, we classified earthquake locations into four quality classes based on the full set of location uncertainties. We observe an increase of high-quality earthquake locations with time, which we attribute to improved network geometry and more precise timing of arrival times. The new earthquake locations show tighter clustering of epicenters and focal depths when compared with original earthquake locations obtained from linearized earthquake location using one-dimensional velocity models. No significant systematic shift, that is, larger than the average location error of a few kilometers, is observed between relocated and original earthquake locations, but we observe large shifts for individual earthquake locations, in particular, for earthquakes of poor location quality. A detailed analysis of the seismicity pattern in Yellowstone is beyond the scope of this study, but we give a general overview and interpretation of the relocated seismicity.

Seismic Networks in Yellowstone

Between 1972 and 1981, the U.S. Geological Service (USGS) operated analog seismic stations in Yellowstone (Pitt, 1987). The number of stations and the geometry of the network varied considerably through time. The largest extent of the network and the highest number of 26 stations was achieved in October 1974 (Fig. 2a). All stations were equipped with 1-Hz vertical seismometers. Data were tele-

metered by radio and telephone lines to Mammoth Hot Springs in Yellowstone; after 1979, data were telemetered to the USGS in Menlo Park, California. P- and S-wave arrival times were manually picked on Develocorder films. Earthquake locations were calculated with the computer program HYPO71 (Lee and Lahr, 1972) using a one-dimensional velocity model and associated station corrections. Pitt (1987) published earthquake locations between 1972 and 1981.

In November 1981, the Yellowstone seismic network was reduced to two helicorders (with paper reading only) located at Old Faithful and Mammoth Hot Springs visitor centers. In November 1983, operation of the Yellowstone seismic network was resumed with 16 stations maintained by the USGS (Fig. 2b). Data were telemetered to the University of Utah Seismograph Station (UUSS) located in Salt Lake City, Utah. Complete maintenance and recording of the Yellowstone seismic network was transferred to the UUSS in 1991 (Nava and Smith, 1996). Between 1983 and 1994, all stations were equipped with 1-Hz vertical component seismometers (Fig. 2b). Arrival times were digitally picked using the computer program PING and an observational weight ranging from 0 to 4 was assigned to each observation based on picking uncertainties. Earthquake locations were obtained by using the computer program HYPOINVERSE (Klein, 1978). A one-dimensional velocity model (Richins *et al.*, 1985) based on the analysis of the 1983 Borah Peak, Idaho, sequence recorded at several seismic refraction profiles near Mackay, Idaho, was used to locate earthquakes between 1983 and 1987. In 1988, a subset of 893 high-quality, that is, well observed, earthquakes between 1983 and 1987 was selected to determine a one-dimensional P- and S-wave velocity structure and P- and S-wave station corrections (Nagy and Smith, 1989a). This ve-
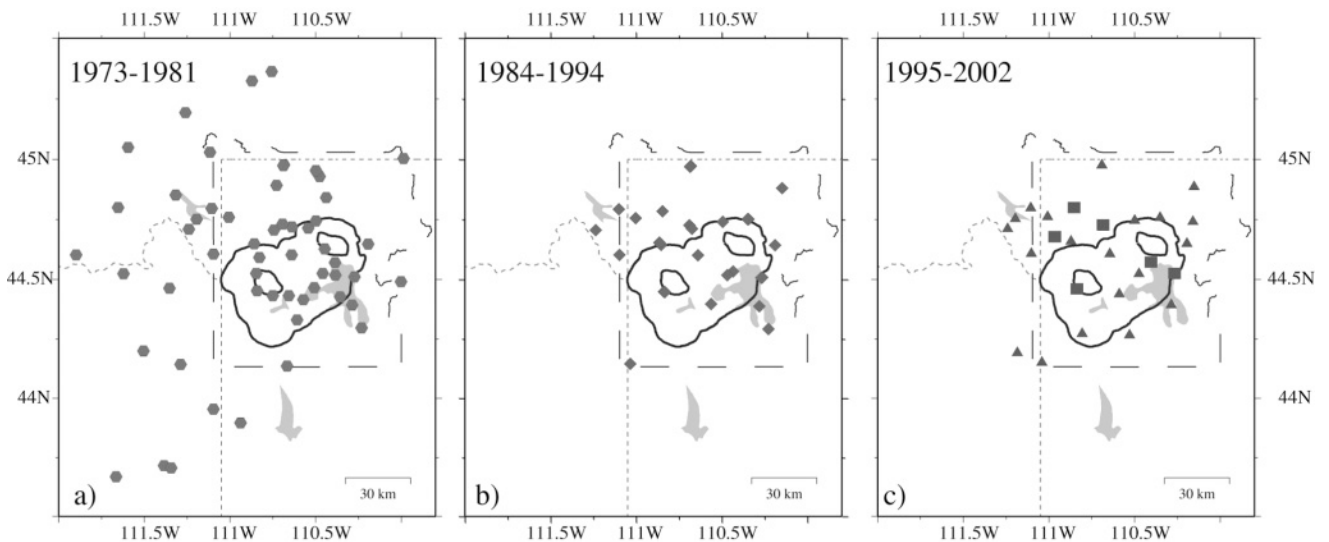

Figure 2.   Seismic network layouts for three-different time periods in the Yellowstone National Park region. Seismic stations are shown by different symbols for different time periods. Black squares denote three-component seismometers; all other symbols denote one-component seismometers.

locity model has been used since 1988 to locate earthquakes in Yellowstone. Since 1992, station corrections have not been used because of the installation of new stations. Earthquake locations between 1984 and 1994 were published in yearly reports by the UUSS (Smith, 1985, 1986; Smith and Nagy, 1987; Nagy and Smith, 1989a, b; Peyton and Smith, 1990; Hardman and Smith, 1991; Nava and Smith, 1993, 1996).

Since 1995, yearly upgrades of the Yellowstone network has increased the number of three-component stations. By the end of 2002, six three-component seismometers were operating in Yellowstone, four of which were broadband seismometers (Fig. 2c). In addition, 19 stations with 1-Hz one-component seismometers were operating. All data are telemetered to the UUSS via analog telemetry except for data from three broadband seismometers that are digitally telemetered. Since 1995, no changes were made to data-processing and earthquake location procedures.

Three-dimensional Velocity Models for Earthquake Locations

Local earthquake tomography is a natural approach to determine reliable three-dimensional velocity models for earthquake locations. Numerous applications of local earthquake tomography to relocate earthquakes exist (e.g., Miller and Smith, 1999; Hauksson, 2000; Hole *et al.*, 2000; Husen *et al.*, 2003a). Because of the long time span from 1973 to 2002 and active tectonic processes taking place in Yellowstone, we decided to split the period from 1973 to 2002 into three individual periods: 1973–1981, 1984–1994, and 1995–2002, representing three periods of distinct network configuration and deformation. During the first period the USGS operated the network, and earthquake data were analyzed at Menlo Park, California; the second period marks the transition from the USGS to the UUSS being responsible for the Yellowstone network; and during the last period, the network was in full operation and additional *S*-wave data were available. The three different periods also correspond to different cycles of crustal deformation observed in Yellowstone. Uplift of up to 1 m was predominant from 1923 to 1984 as determined by leveling data (Pelton and Smith, 1979; Dzurisin *et al.*, 1994). A rapid change to caldera-wide subsidence was detected in 1985 that exceeded 25 cm by 1995 (Dzurisin *et al.*, 1994). Interferometric synthetic aperture radar (InSAR) and Global Positioning System (GPS) measurements revealed a partial return to uplift in the northwest part of the caldera that started 1995 and continued to 2002 (Wicks *et al.*, 1998; Meertens *et al.*, 2000). It is possible that these different deformation cycles may have changed the seismic velocity structure beneath Yellowstone.

Earthquake data were selected for each of the periods just discussed, applying the same selection criteria and inverting separately for seismic velocities and hypocenter locations. Because of the inherent coupling between seismic velocities and hypocenter locations only highest-quality

data, as described subsequently, were used. Prior to data selection, all earthquakes between 1973 and 2002 were relocated by using a minimum one-dimensional model (Kissling *et al.*, 1994) and corresponding station delays. The minimum one-dimensional model was obtained by inverting a subset of 482 high-quality, that is, with at least 12 observations and an azimuthal gap <120°, earthquakes from 1995 to 2002 for one-dimensional *P*- and *S*-wave velocities and station delays. The validity of the minimum one-dimensional model was checked for the earlier times and new station delays were computed by inverting for *P*-wave velocities and station delays for each period by using the *P*-wave velocities of the 1995–2002 minimum one-dimensional model as initial velocities. Only small changes in velocities were observed, indicating that the average one-dimensional velocity structure in Yellowstone did not change notably with time. Table 1 lists velocities of the minimum one-dimensional model from 1995 to 2002 that was used as initial reference model for the following three-dimensional inversion for all times.

After relocation, earthquake data were selected for each period by applying the following selection criteria: (1) at least eight observations, (2) at least one observation within 1.5 focal depth distance, (3) an azimuthal gap <180°, and (4) an event root mean square (rms) <0.5 sec. Table 2 lists the number of earthquakes and observations selected for each period. The highest number of data were available between 1995 and 2002 when the Yellowstone network was fully operational and data loss was low. Instrument mal-

Table 1
Minimum One-Dimensional Velocity Model as Obtained by Simultaneous Inversion of Velocities and Earthquake Locations from 482 High-Quality Earthquakes between 1995 and 2002

Depth (km)	*P*-Wave Velocity (km/sec)	*S*-Wave Velocity (km/sec)
−4.0 (above sea level)	2.76	1.38
0.0	5.05	2.58
2.0 (below sea level)	5.35	3.35
4.0	5.40	3.35
6.0	5.41	3.40
8.0	5.89	3.45
10.0	5.96	3.46
12.0	6.05	3.46
14.0	6.14	4.54
18.0	6.50	4.54

Table 2
Number of Earthquakes and Observations Used in Tomographic Inversion for Each Time Period

Time Period	Number of Earthquakes	Number of Observations
1973–1981	1313	14,459
1984–1994	609	5,590
1995–2002	3374	34,538 *P*
		5,875 *S*

functions were highest between 1984 and 1994 resulting in the lowest number of available data. Varying station configurations and a high number of events with rms >0.5 sec reduced the number of available data between 1973 and 1981. The abnormally high number of events with rms > 0.5 sec between 1973 and 1981 may have been caused by timing problems of the seismic data, as discussed below. Because of the lack of three-component seismometers no reliable S-wave data were available before to 1994.

We used the computer code SIMULPS14 (Thurber, 1983; Eberhart-Phillips, 1990), extended by Haslinger and Kissling (2001) for full three-dimensional ray shooting, to invert simultaneously for hypocenter locations and three-dimensional P-wave velocity (V_P), and P-wave to S-wave ratio (V_P/V_S) structure. Because of the lack of S-wave data, we inverted for V_P/V_S only for the time 1995–2002. The method inverts S–P arrival times for V_P/V_S by projecting S–P arrival time residuals into V_P/V_S variations (Thurber and Atre, 1993). S- and P-arrival time residuals are computed by three-dimensional ray tracing through the corresponding velocity models; the necessary S-wave velocity model is derived from the V_P and V_P/V_S models. SIMULPS14 solves the nonlinear, coupled hypocenter-velocity problem by a linearized, iterative, damped least-square scheme. Each iteration consists of an inversion for V_P and optionally V_P/V_S variations, and for hypocenter locations. Damping values were selected to be 500 for all inversions by analyzing trade-off curves between model variance and data variance (Eberhart-Phillips, 1986). The chosen damping values provided the largest reduction in data variance without increasing model variance strongly, hence yielding the smoothest solution to fit the data.

Velocity models for all three periods were parameterized by a horizontal grid node spacing of 15 × 15 km; grid nodes in vertical direction were positioned at −4.0 km (above sea level), −1.0 km, 2.0 km (below sea level), 5.0 km, 8.0 km, 12.0 km, 16.0 km, and 21.0 km. The high number of P-wave arrivals between 1995 and 2002 would support finer grid spacing for the V_P model, in particular, in the northwestern part of the model, but the low number of S–P arrivals did not. After five iterations, each of the inversions achieved a reduction in data rms and data variance shown in Table 3. All the inversions achieved a similar reduction in data variance; the slightly lower reduction in variance between 1984 and 1994 indicates that a larger part of three-dimensional structure cannot be resolved by this data set, possibly due to the lower number of observations. As shown in Table 3, initial and final rms between 1973 and 1981 is twice as large as those between 1984 and 2002. This clearly reflects higher uncertainties in the arrival times, possibly related to picking those data on analog Develocorder films.

We do not give a detailed interpretation of the different velocity models (Fig. 3), because that is beyond the scope of this study. A common feature of all three velocity models is reduced P-wave velocities beneath the Yellowstone caldera at depths greater than 5.0 km. These low velocities may

Table 3
Data rms and Data Variance Reductions after Tomographic Inversion

Time Period		Data rms (sec)	Data Variance (sec)	Reduction (%)
1973–1981	Initial	0.404	0.188	58
	Final	0.259	0.109	
1984–1994	Initial	0.233	0.065	48
	Final	0.125	0.031	
1995–2002	Initial	0.189	0.055	62
	Final	0.116	0.021	

Each inversion consists of five iterations.

represent a region of hot, crystallizing magma (Miller and Smith, 1999). It is noteworthy, however, that we observe differences in the V_P structure between the different time periods (Fig. 3). A detailed interpretation of the three-dimensional V_P and V_P/V_S structure of Yellowstone between 1995 and 2002 was given by Husen et al. (2004). Previous tomographic studies in Yellowstone were interpreted by Benz and Smith (1984) and Miller and Smith (1999).

Three-dimensional Probabilistic Earthquake Location

Method

In this study we used the software package NonLinLoc (Lomax et al., 2000) to relocate the Yellowstone earthquake catalog from 1973 to 2002. NonLinLoc follows the probabilistic formulation of nonlinear inverse problems by Tarantola and Valette (1982). A complete description of this formulation can be found in Tarantola and Valette (1982) and Moser et al. (1992). Therefore, we present only a short summary of the basic ideas. The probabilistic formulation of nonlinear inverse problems relies on the use of normalized and unnormalized probability density functions to express our knowledge about the values of parameters. If the probability density functions giving a priori information on the model parameters and on observations are independent, and the theoretical relationship relating a vector of observed data and unknown parameters can be expressed as a conditional density function, then a complete, probabilistic solution can be expressed as a posteriori probability density function (PDF) (Tarantola and Valette, 1982). In earthquake location, the unknown parameters are the hypocentral coordinates (x, y, and z) and the origin time T, the observed data are arrival times measured at seismograph stations, and the theoretical relation gives predicted or theoretical travel times. If the theoretical relationship and the observed travel times are assumed to have Gaussian uncertainties expressed by covariance matrices, and if the a priori information on the origin time is taken as uniform, the PDF can be evaluated analytically in a marginal PDF for the spatial location and the origin time (Tarantola and Valette, 1982; Moser et al., 1992).

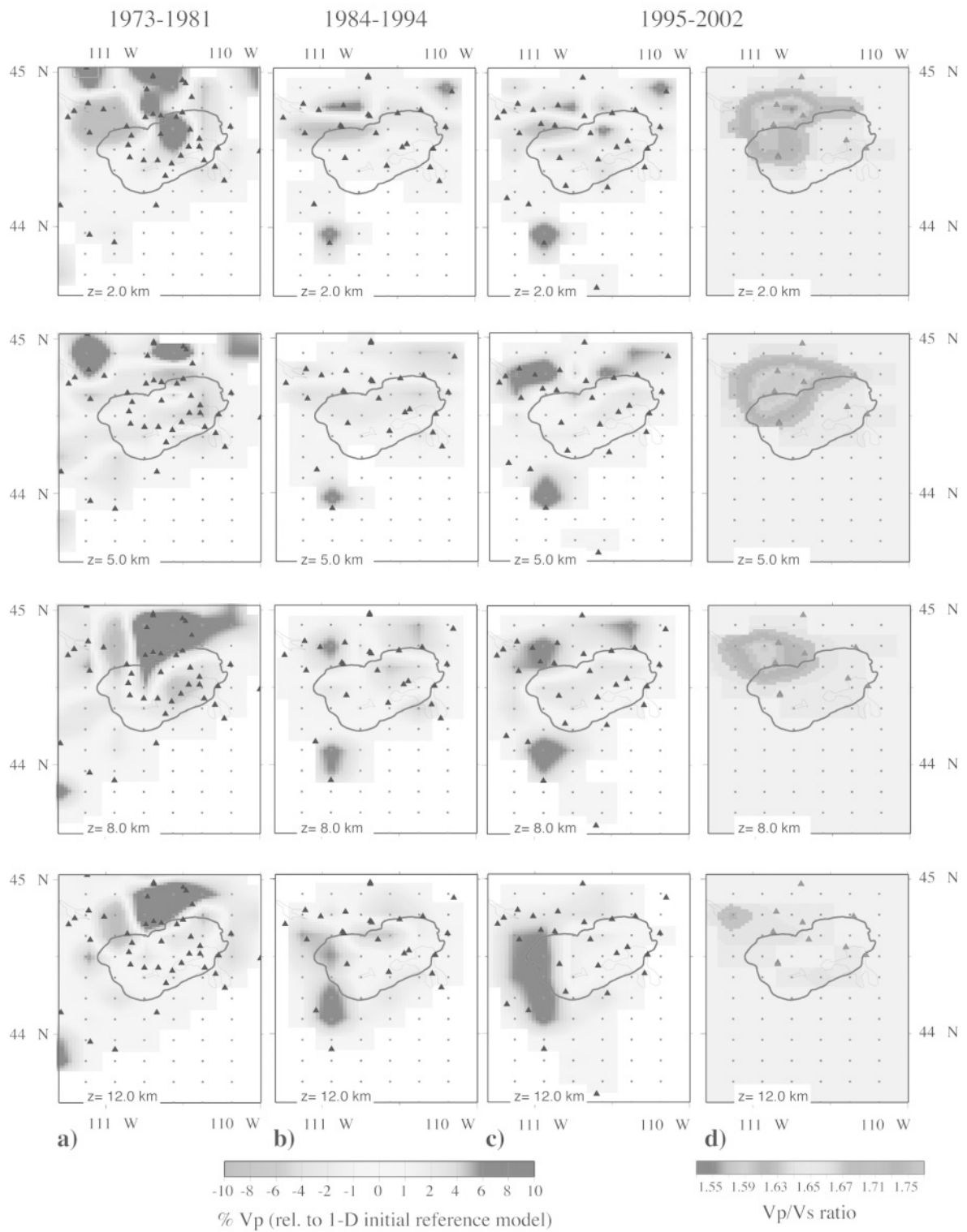In NonLinLoc, the PDF can be computed in three

Figure 3. Tomographic velocity models for three time periods: (a) 1973–1981, (b) 1984–1994, and (c, d) 1995–2002. Velocity models are shown in plane views at four different depths. Areas that are not resolved are shown in white. Dots mark position of velocity grid nodes. Triangles mark seismic stations used in the inversion. Outline of the Yellowstone caldera is shown by a thick black line. *P*-wave velocity models are shown as percentage change relative to one-dimensional initial reference model of the inversion; model of *P*-wave to *S*-wave ratio (V_P/V_S) is shown by absolute values.

different ways (Lomax *et al.*, 2000): (1) via a grid-search algorithm using successively finer, nested grids; (2) via a Metropolis-Gibbs sampling algorithm performing a directed random walk within a spatial volume to obtain a set of samples that follow the PDF; and (3) via an Oct-Tree Importance sampling algorithm (Oct-Tree algorithm). The Oct-Tree algorithm gives accurate, efficient and complete mapping of the PDF of the earthquake location problem (Lomax and Curtis, 2001). It uses recursive subdivision and sampling of cells in three dimensions to generate a cascade of sampled cells, where the number of sampled cells follows the values of the PDF at the cell center, thus leading to higher density of cells in areas of higher PDF (lower misfit). Multiple minima in the PDF are reliably detected by the grid-search algorithm and the Oct-Tree algorithm but are missed by the Metropolis-Gibbs sampling algorithm. The Oct-Tree algorithm outperforms the grid-search algorithm by a factor of 100 in computing time (Lomax and Curtis, 2001); however, the Oct-Tree algorithm may not detect narrow, local minima in the PDF.

Location Uncertainties

The PDF represents a complete, probabilistic solution to the location problem, including information on uncertainty and resolution (Lomax *et al.*, 2000). The solution is fully nonlinear, and, therefore, the resulting PDF may be irregular and multimodal. The solution includes location uncertainties due to the geometry of the network, measurement errors of the observed arrival times, and errors in the calculation of the theoretical travel times. Realistic estimates of the errors must be specified in a Gaussian form through covariance matrices. For example, measurement errors can be presented in the form of a weighting scheme, assigning each weight a certain travel time uncertainty. The specific inclusion of error estimates through covariance matrices and the fully nonlinear solution makes probabilistic earthquake location superior to traditional linearized earthquake location. It is important, however, to note that the uncertainties included in the solution are only relative, unless one is able to estimate travel time errors due to incorrect velocity structure in a Gaussian form (Lomax *et al.*, 2000).

Location uncertainties of probabilistic earthquake location are often shown as confidence volumes or confidence contours (Fig. 4a) (Moser *et al.*, 1992; Lomax *et al.*, 2000), which can be estimated from the PDF. This is only possible, however, if the complete PDF is available, as obtained by the grid-search algorithm. In global sampling methods such as the Metropolis-Gibbs sampler or the Oct-Tree algorithm, the complete PDF is not available and location uncertainties are shown by density plots (Fig. 4b). These density plots are obtained by drawing samples from the PDF with the number of samples proportional to the probability (Lomax *et al.*, 2000). In both cases, the final hypocenter location is given by its maximum likelihood value (Fig. 4, star). In addition to the location uncertainties included in the probabilistic solution to the location problem, NonLinLoc produces tradi-

tional Gaussian estimates such as the expectation hypocenter location (Fig. 4, circle) and the 68% confidence ellipsoid (Lomax *et al.*, 2000). These estimates may be interpreted as results obtained by linearized location algorithms such as HYPO-71 (Lee and Lahr, 1972) or HYPOINVERSE (Klein, 1978).

Application to Yellowstone Earthquake Catalog

For this study we used the Oct-Tree algorithm because it gives accurate and reliable mapping of the PDF, thereby being more efficient than a grid-search algorithm. Identical parameters for the Oct-Tree algorithm, that is, the number of initial and final cells, are used through the entire study. Analyzing scatter plots of each of the 25,267 earthquakes to determine the location quality proved impractical. We therefore classified all earthquakes in four quality classes A, B, C, and D (Table 4). Figure 5 shows example scatter plots for each quality class. Definition of the quality classes is based on a comprehensive set of uncertainty parameters computed by NonLinLoc. One parameter that proves to be important is the difference between the maximum likelihood and expectation hypocenter locations. Large differences between the maximum likelihood and the expectation hypocenter locations can result from an ill-conditioned location problem (Lomax *et al.*, 2000). In this case, Gaussian location estimates, such as the confidence ellipsoid, are no longer adequate uncertainty estimates because location uncertainties can be strongly irregular (Fig. 5c) or show multiple minima.

Between 1973 and 1981 we found a high percentage (Fig. 6) of earthquakes having a rms > 0.5 sec. These large rms values, as compared with the final rms of the tomographic velocity model, are caused by a large number of observations having residuals of >1.0 sec (Fig. 5d). We suggest that these large residuals could be either caused by mispicked arrival times or by timing problems of the seismic data. In any case, the locations of these earthquakes are not useable. The number of earthquakes having a rms > 0.5 sec decreases to less than 1% between 1984 and 2002 (Fig. 6), indicating a strong improvement in data quality.

The choice of 0.5 km on the difference between maximum likelihood and expectation hypocenter locations for quality class C (Table 4) is somewhat arbitrary. We looked, however, at a large number of scatter plots and all of them indicated that, in general, earthquakes with a difference of >0.5 km had large uncertainties of several kilometers in epicenter and focal depth. Figure 5c shows a typical example of a quality class C earthquake; note the poor approximation of the location uncertainties by the confidence ellipsoid. Earthquake locations in quality class C usually suffered from a low number of observations and/or a poor azimuthal distribution of observations. It is notable, that more than 50% of the earthquake locations between 1984 and 2002 are classified in quality class C (Fig. 6). Many of the earthquakes in Yellowstone are of small magnitude, limiting the number of recording stations. Combined with the relatively sparse dis-
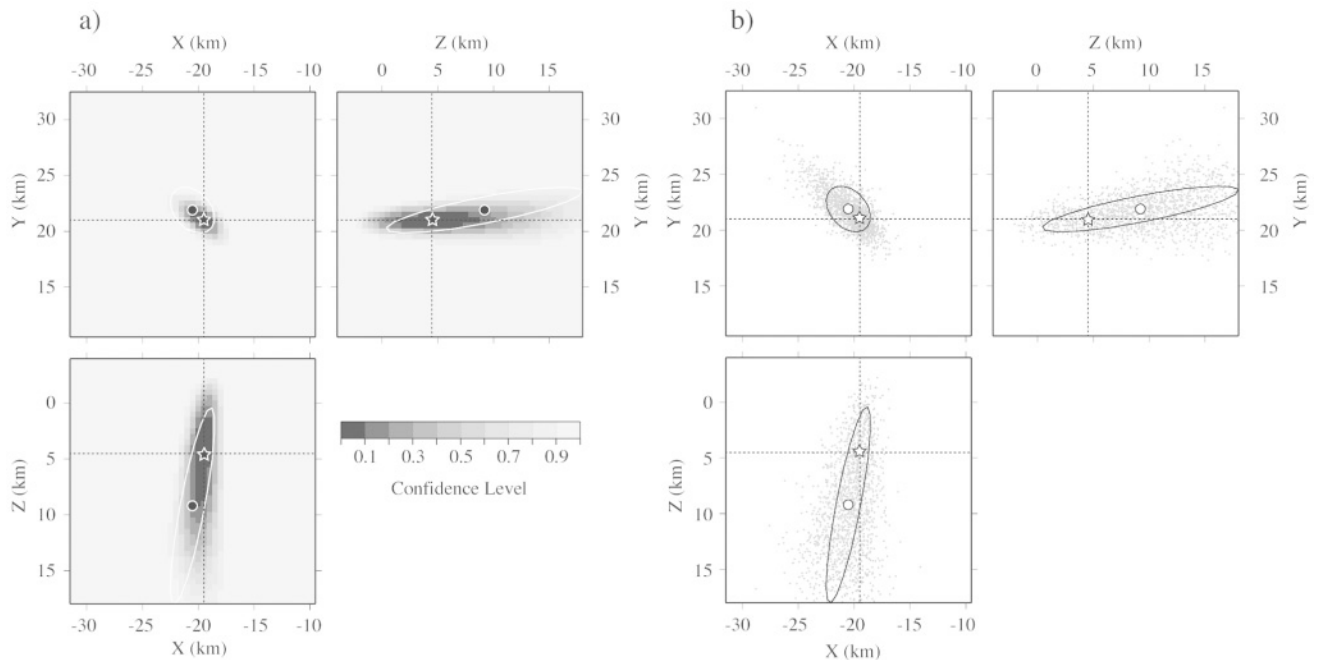
Figure 4. Probabilistic location uncertainties shown by confidence levels (a) and by density scatter plots (b) Plane view in *x–y* direction and cross sections in *x–z* and *y–z* directions are shown. Stars indicate maximum likelihood hypocenter location; circles show expectation hypocenter locations. Projection of the 68% confidence ellipsoid is shown as a white (a) or a black line (b), respectively.

Table 4
Definition of Quality Classes for Earthquake Locations of the Yellowstone Earthquake Catalog

Quality Class	Selection Criteria
A (excellent)	rms < 0.5 sec, DIFF < 0.5 km, average error < 2.0 km
B (good)	rms < 0.5 sec, DIFF < 0.5 km, average error ≥ 2.0 km
C (questionable)	rms < 0.5 sec, DIFF ≥ 0.5 km
D (poor)	rms ≥ 0.5 sec

DIFF corresponds to difference between maximum likelihood and expectation hypocenter locations. Average error is the average length of the three axes of the 68% error ellipsoid.

tribution of stations, this results in a poor azimuthal distribution of observations for these earthquakes.

Most reliable earthquake locations can be found in quality classes A and B. These earthquake locations have a well defined PDF with a single minimum, thus the confidence ellipsoid is a good approximation to the location uncertainties (Fig. 5a,b). We define the average error used to discriminate between quality class A and B (Table 4) by taking the average of the three axes of the 68% confidence ellipsoid. Earthquakes in quality class B usually have well defined epicenter locations, but the focal depth is poorly constrained (Fig. 5b) because of the lack of a station within the critical focal depth distance. This becomes critical for shallow earthquakes, particularly inside the Yellowstone caldera, where shallow earthquakes are abundant and station distribution is

sparser because of logistical difficulties. Earthquake locations classified in quality class A have a very well defined PDF in epicenter and focal depth (Fig. 5a). Consequently, location uncertainties are small, on average < 1.7 km in epicenter and < 3.2 km in focal depth. For the examples shown in Figure 5, the rms for the quality class A location is nearly twice the rms for the quality class B location, which is actually less well constrained. This points out the important fact that rms is a poor measure by which to judge earthquake location quality unless a certain threshold in rms has been determined, based either on *a priori* picking errors or on the final rms of a tomographic inversion, as in this study. The numbers of earthquakes in quality class A show a remarkable increase between 1995 and 2002 as compared with the number of earlier events (Fig. 6). We attribute this improvement to denser station coverage and improvements in network operation since 1995.

Revised Magnitude Calculations

Coda magnitudes (M_c) for 19,097 earthquakes between January 1984 and December 2002 were recomputed using newly available instrument calibrations and an improved coda magnitude equation (Pechmann *et al.*, 2001):

$$M_c = -2.60 + 2.44 \log\tau + 0.0040\Delta, \qquad (1)$$

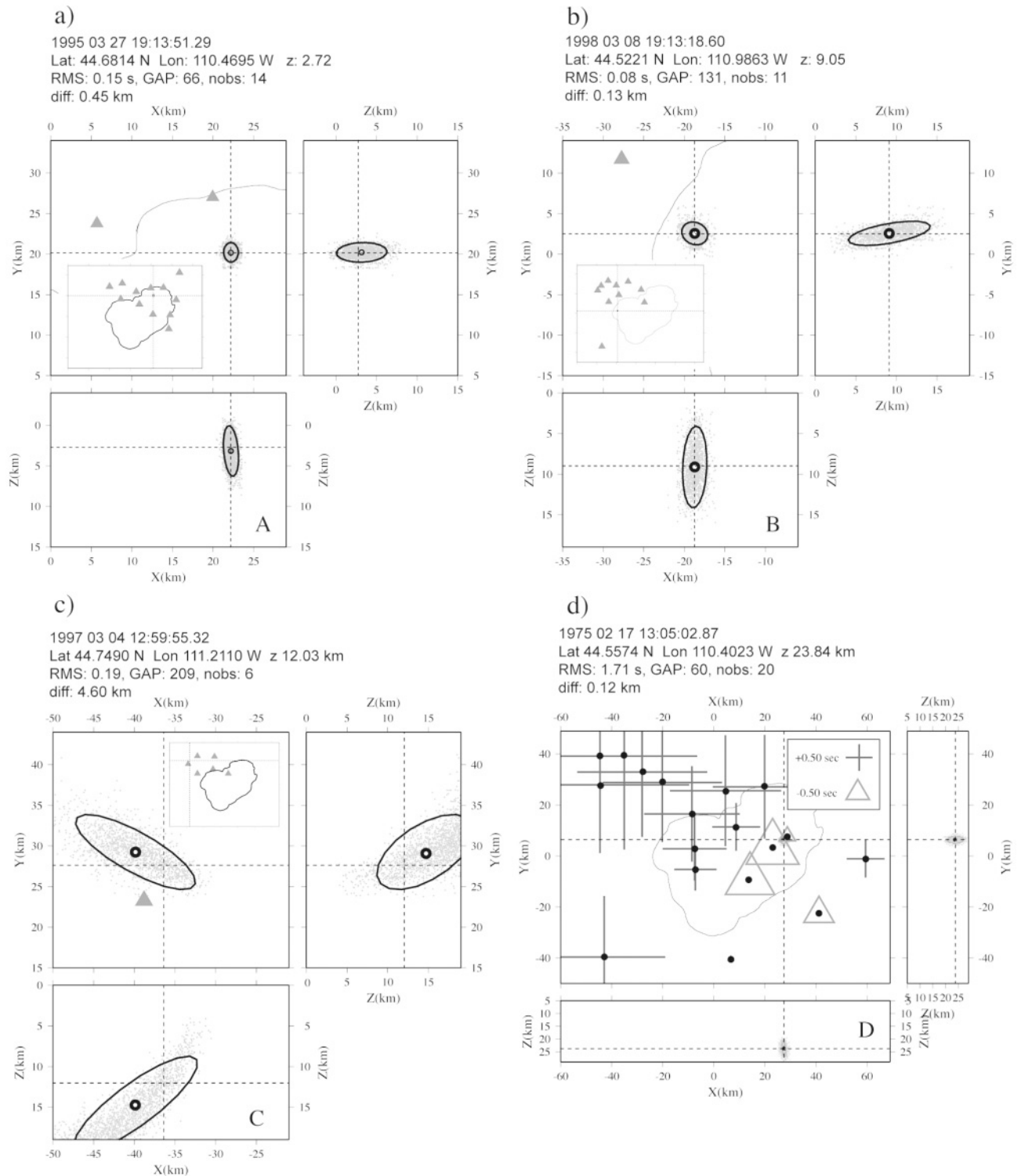where τ is signal duration in seconds measured on a short-

a)
1995 03 27 19:13:51.29
Lat: 44.6814 N Lon: 110.4695 W z: 2.72
RMS: 0.15 s, GAP: 66, nobs: 14
diff: 0.45 km

b)
1998 03 08 19:13:18.60
Lat: 44.5221 N Lon: 110.9863 W z: 9.05
RMS: 0.08 s, GAP: 131, nobs: 11
diff: 0.13 km

c)
1997 03 04 12:59:55.32
Lat 44.7490 N Lon 111.2110 W z 12.03 km
RMS: 0.19, GAP: 209, nobs: 6
diff: 4.60 km

d)
1975 02 17 13:05:02.87
Lat 44.5574 N Lon 110.4023 W z 23.84 km
RMS: 1.71 s, GAP: 60, nobs: 20
diff: 0.12 km

Figure 5.   Density scatter plots of representative earthquakes for each quality class A, B, C, and D defined in this study. Plane view in *x*–*y* direction and cross sections in *x*–*z* and *y*–*z* directions are shown. Maximum likelihood hypocenter location is at the intersection of dashed lines. Circles denote expectation hypocenter location. Projection of the 68% confidence ellipsoid is shown by heavy black lines. Inlays for a, b, and c show on overview of the entire region. Triangles mark the seismic station used to locate earthquake except in d, where seismic stations are shown by crosses and triangles scaled by residuals. Outline of Yellowstone caldera is shown by a thin black line.

period vertical component seismogram, and Δ is epicentral distance in kilometers. Signal duration is measured from the *P*-wave arrival to the time that the seismic signal drops below the noise level, which is defined as 0.01724 µm/sec based on the median noise level for short-period analog-telemetered stations in the UUSS regional seismic network (Pechmann *et al.*, 2001). Equation (1) was modified from existing coda magnitude equations for Yellowstone by (1) using a fixed noise level, which corresponds to a ground velocity of 0.01724 µm/sec for a median 5-Hz gain of a typical high-gain vertical component station in the USS network, instead of pre-event noise level, (2) correcting signal-duration measurements for instrument gain because signal-duration measurements are done relative to a median 5-Hz gain, (3) fixing a relatively minor coding error in the UUSS software for automatically determining signal durations, and (4) calibrating M_L against Richter local magnitudes M_L (Richter, 1958) over a wider distance and magnitude range. The latter data set encompassed 510 earthquakes in the Yellowstone region with M_L ranging from 0.6 to 4.2. The new coda magnitude equation (1) improves average $M_c - M_L$ differences to less than M 0.1 for $M_L < 4.0$ events compared with previous systematic time-dependent $M_c - M_L$ differences ranging up to M 1.0 (Pechmann *et al.*, 2001). Consequently, the revised coda magnitudes computed by equation (1) are similar to local magnitudes.

Final coda magnitudes in the Yellowstone earthquake catalog are the average of at least three coda magnitude estimations at three different stations. Coda magnitudes determined from two or fewer are not reliable. Therefore, coda magnitudes of these earthquakes were set to -9.90, so that the hypocenter locations can still be used but the magnitude is marked as unreliabe. We screened and removed average M_c estimations for outliers, that is, individual M_c values larger then one magnitude unit from the mean, which are consequently removed. This process was iteratively repeated until no more outliers were found. If during this process the number of individual M_c estimations for one earthquake fell below 3, the coda magnitude for that earthquake was set to -9.90.

Recomputed magnitudes are consistently smaller by M 0.8. Due to the removal of previous systematic time-dependent magnitudes shifts, our recomputed coda magnitudes are more consistent and reliable. Moreover, with the new coda magnitude equation negative M_c values are allowed, which previously were set to zero and discarded. Average M_c between 1984 and 2002 is 0.9, and only 6% of the earthquakes have $M_c > 2.0$ (Fig. 7).

Discussion

Differences Between Routine and NonLinLoc Probabilistic Earthquake Locations

Figure 8 shows differences in hypocenter locations between original hypocenter locations obtained routinely by
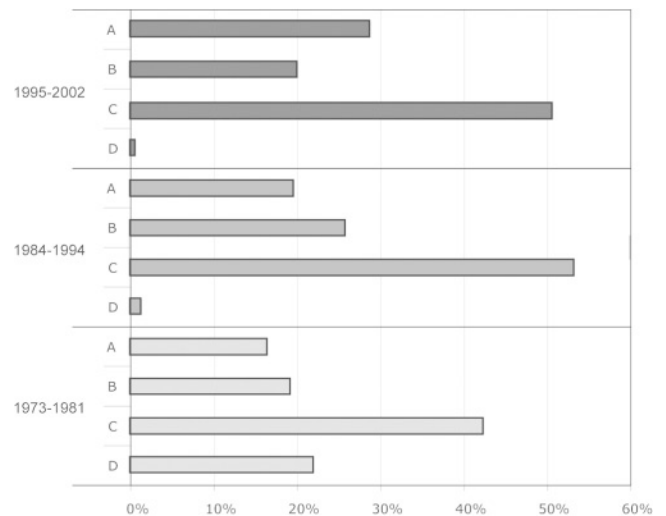
Figure 6.   Percentage of earthquakes for each quality class defined in this study and each time period.
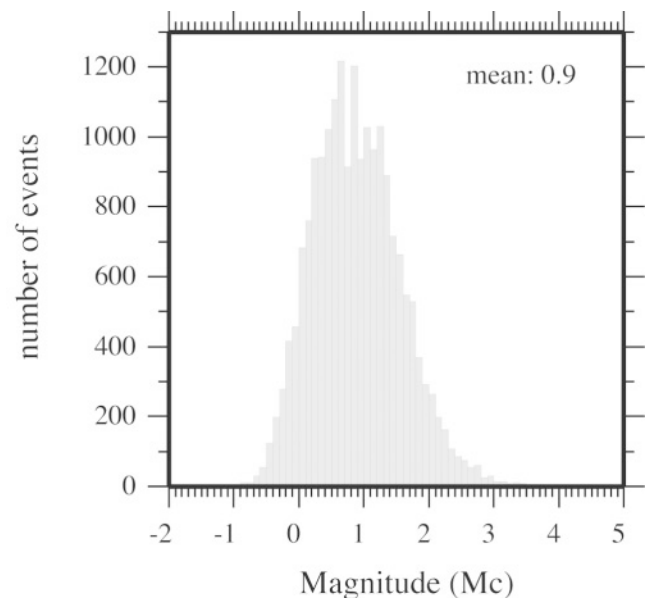
Figure 7.   Histogram of magnitudes recomputed in this study for earthquakes between 1984 and 2002.

using linearized earthquake location and one-dimensional velocity models and relocated earthquake locations obtained in this study. No systematic shifts in longitude and latitude are observed between original and revised earthquake locations. However, large individual shifts in longitude and latitude are observed. These shifts are larger for latitude and for earthquakes of quality C and D. Larger shifts in latitude are a consequence of the network geometry because more stations exist in east-west direction than in north-south direction (Fig. 2). Larger individual shifts for quality C and D earthquakes clearly reflect poorer location quality of these events. Earthquakes of quality class A and B have well con-
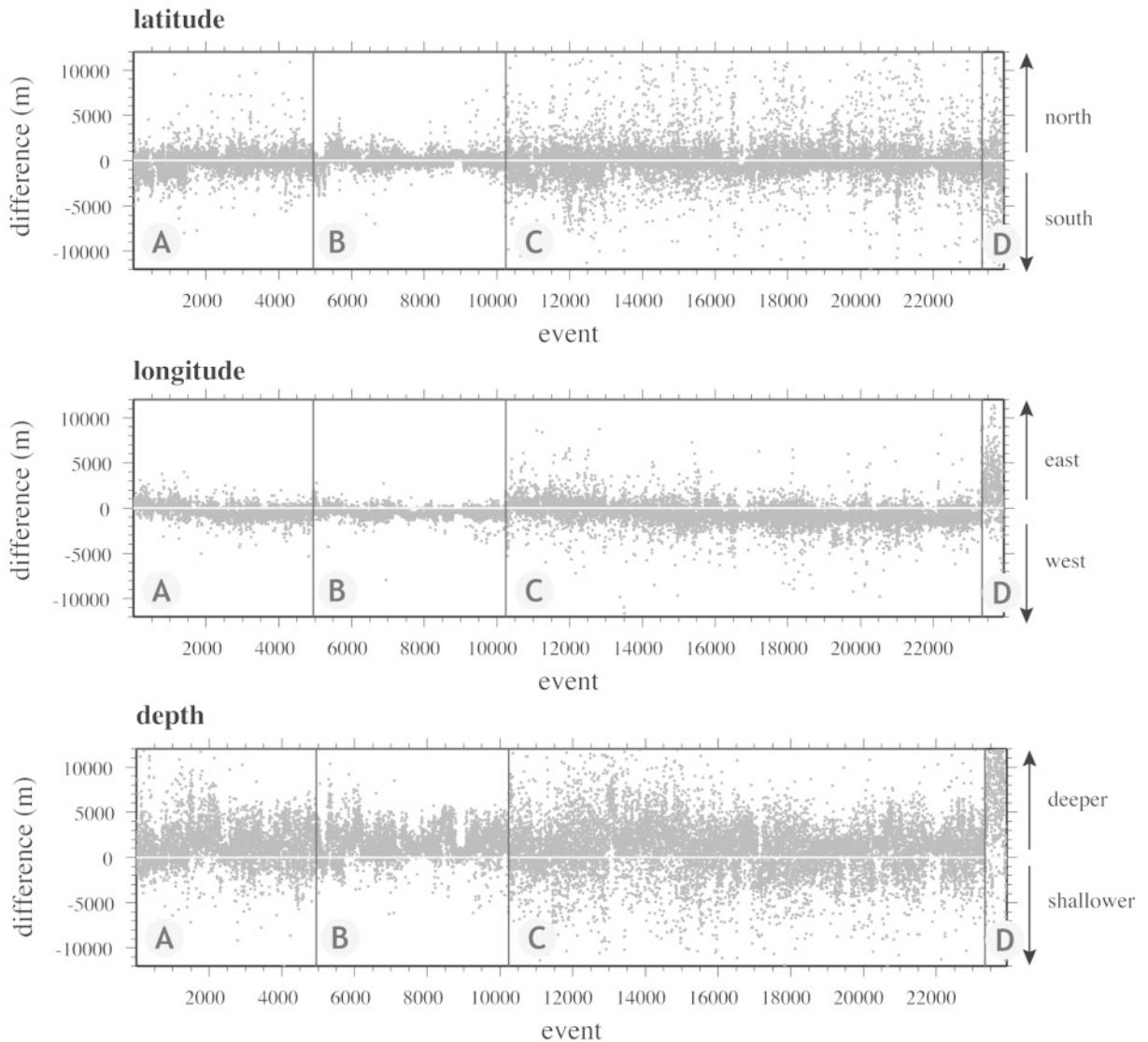
Figure 8.   Differences in depth, latitude, and longitude between UUSS routine earthquake locations and relocated NonLinLoc earthquake locations between 1995 and 2002. UUSS earthquake locations were obtained by linearized earthquake location using one-dimensional velocity models; NonLinLoc earthquake locations were obtained by probabilistic earthquake location and three-dimensional velocity models. Earthquakes were grouped into quality classes as indicated by letters. Arrows show the direction of the shift of NonLinLoc earthquake locations relative to UUSS earthquake locations.

strained epicenter locations as opposed to earthquake of quality C and D (Fig. 5).

Relocated earthquakes are on average ~2 km deeper than original hypocenter locations (Fig. 8). Large individual shifts (>5 km) are observed for earthquakes of all quality classes, but in significantly greater number for quality C and D earthquakes (Fig. 8). Shallow low V_P velocities in the northwestern part of the tomographic model area (Fig. 3) likely cause a systematic shift to greater depth for earthquakes relocated in this study. Seismicity is most intense in this region and resolution of the tomographic models is highest for this area, thus velocities in this region are well con-

strained. These low velocities are obviously not detected using one-dimensional velocity models.

Our relocated earthquakes show a seismicity pattern that is more focused and shows more detail (Fig. 9 and 10). This becomes particularly evident in a vertical cross section (Fig. 10). Relocated focal depths cluster more tightly over a range of 8 km (between 2 km and 10 km depth), whereas original focal depths spread over a range of 12 km (between 2 km above sea level and 10 km depth). Because we observed only a relatively small systematic shift of ~2 km to greater depth and maximum depth of seismicity remained unchanged, most of the shallow seismicity was moved to greater depth
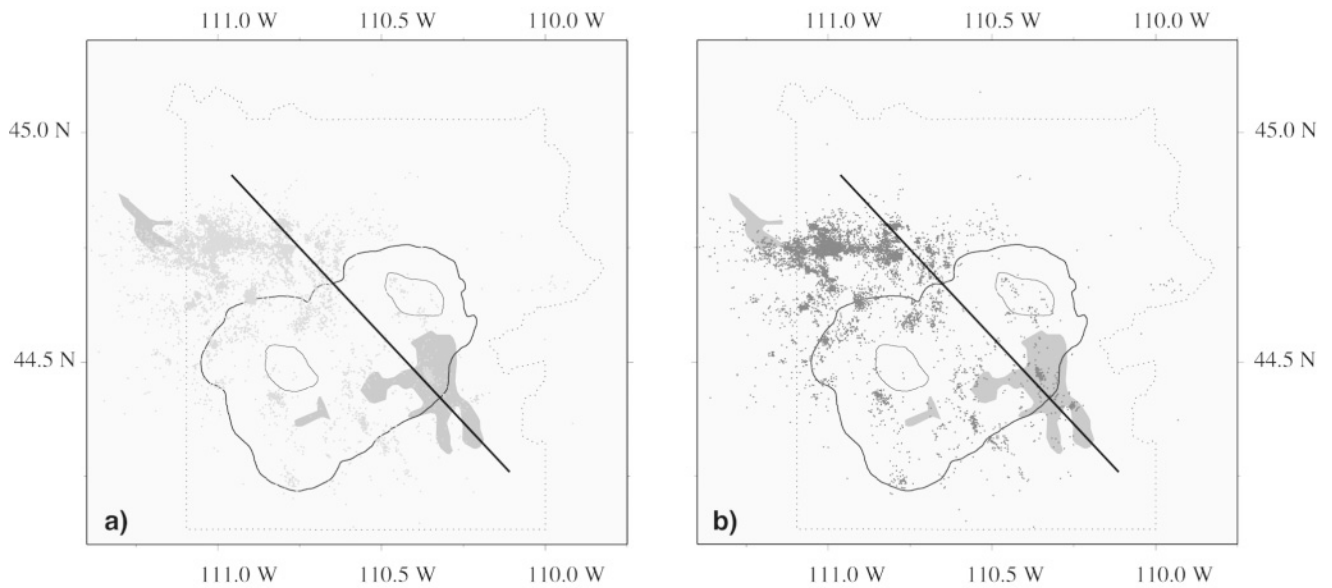
Figure 9. Epicenter locations between 1973 and 2002 obtained by linearized earthquake location using one-dimensional velocity models (a) and obtained by probabilistic earthquake location using three-dimensional velocity models (b). Only well located earthquakes (quality classes A and B) are shown. Location of cross section in Figure 10 is shown by thick black line. Caldera boundary and resurgent domes are outlined by a thin black line. Dashed line marks boundary of Yellowstone National Park.
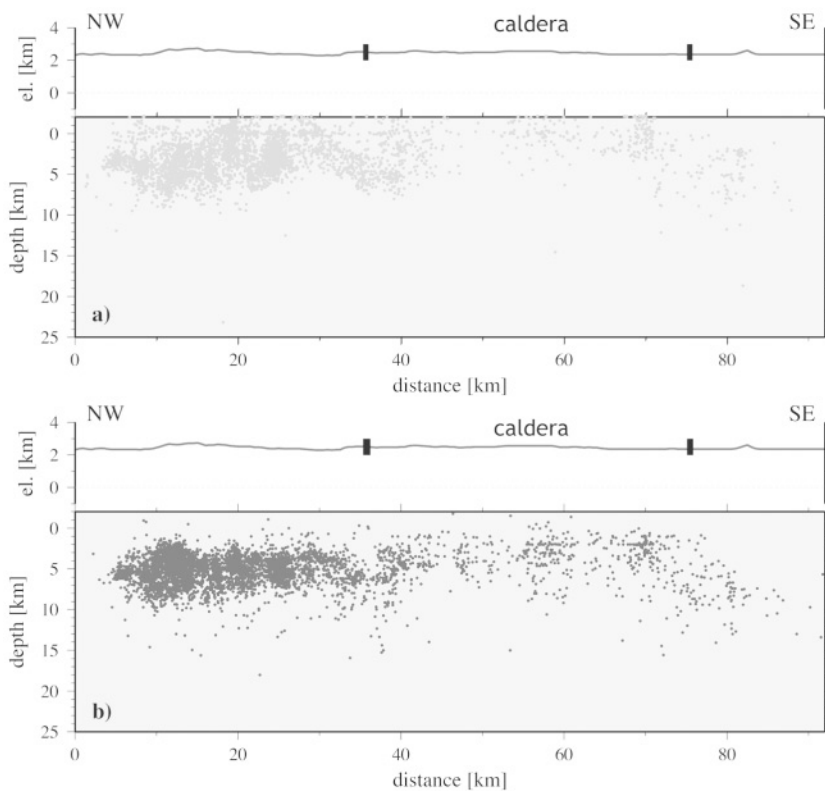

Figure 10. Same as Figure 9 except for the vertical cross section. See Figure 9 for profile location. Cross sections are 20 km wide. Topography along profile is shown on the top. Rectangles mark intersection of profile with caldera boundary.

when relocated. Shallow events are difficult to locate because a reliable focal depth estimate requires a station within focal depth distance. This suggests that probabilistic earthquake location provides more consistent and reliable focal depths than linearized earthquake location.

Seismicity Patterns in the Yellowstone Region

Within the scope of this study we can only give a brief description of seismicity patterns and their interpretation in the Yellowstone region. Relocated hypocenter locations from 1973 to 2002 are shown in map view (Fig. 11) and along three vertical cross sections (Fig. 12). As one of the possible applications taking advantage of improved hypocenter locations and magnitudes, we computed the cumulative seismic moment release in the Yellowstone region from 1984 to 2002 (Fig. 13). We were not able to compute the seismic moment release prior to 1984 because no information on station calibrations is available for this early time period. We converted coda magnitudes into seismic moment using the relationships given in Table 5.

Most well constrained earthquake locations (class A and B) are located in the northwestern part of the Yellowstone region between Hebgen Lake and the northern rim of the Yellowstone caldera and inside the Yellowstone caldera (Fig. 11). To the east and to the south of the Yellowstone caldera hypocenter locations are less well constrained due to the lack of seismic stations. In general, shallow seismicity (< 2.0 km depth) is poorly constrained unless a seismic station lies within focal depth distance, which is the case for some hydrothermal areas such as Upper Geyser Basin, West Thumb Geyser Basin, and Norris Geyser Basin (Fig. 12). A relatively large number of earthquakes located in the northeastern part of the caldera have unrealisticly large focal depths (Fig. 11 and 12). These earthquakes occurred mostly between 1973 and 1981 and had very large rms (>1 sec) caused by a high number of residuals >1 sec, which makes
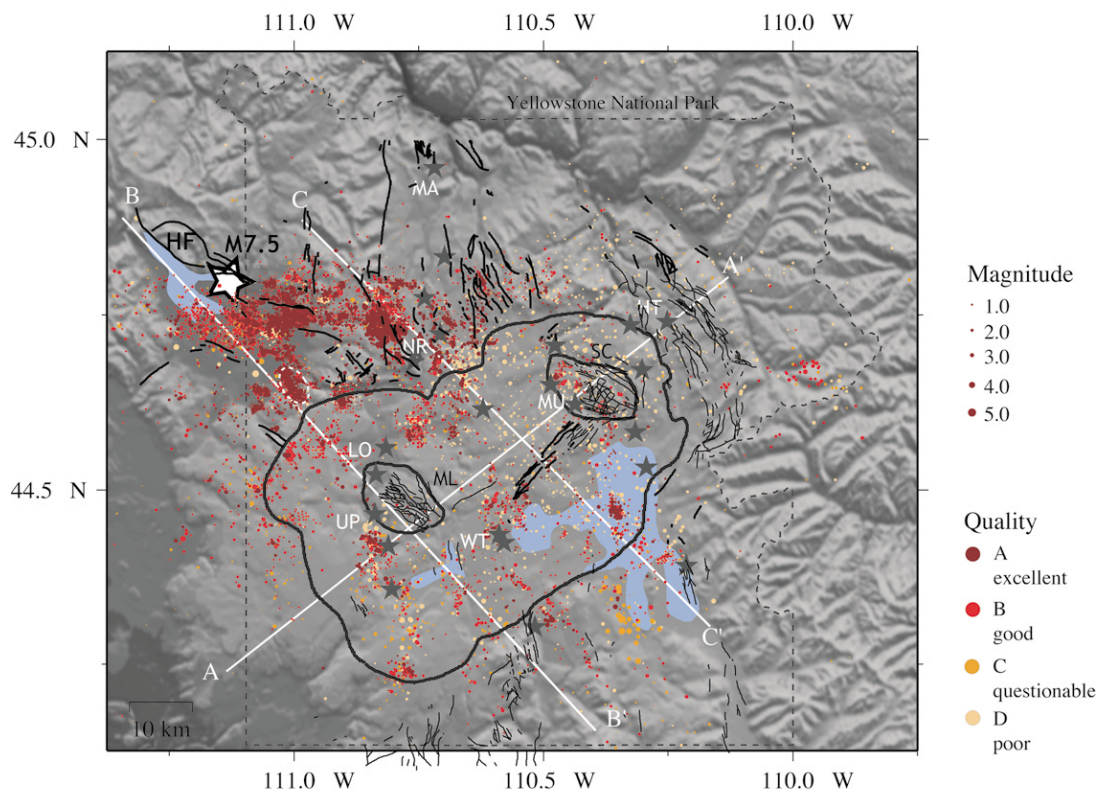

Figure 11.   Revised earthquake locations of this study for the Yellowstone National Park region obtained by probabilistic earthquake location using three-dimensional velocity models. Earthquake locations are color coded by quality and scaled by magnitude. Large star marks location of the M 7.5 1959 Hebgen Lake earthquake. Area of the 1985 earthquake swarm is marked by white, dashed ellipse. Thick black lines outline Yellowstone caldera and resurgent domes: ML, Mallard Lake; SC, Sour Creek. Thin black lines mark mapped Quaternary faults. Gray stars denote mapped hydrothermal features; major hydrothermal features are labeled. HT, Hot Springs Basin; MU, Mud Volcano; WT, West Thumb Geyser Basin; UP, Upper Geyser Basin; LO, Lower Geyser Basin; NR, Norris Geyser Basin; MA, Mammoth Hot Springs. Cross sections shown in Figure 10 are outlined by white lines. HF, Hebgen Lake fault.
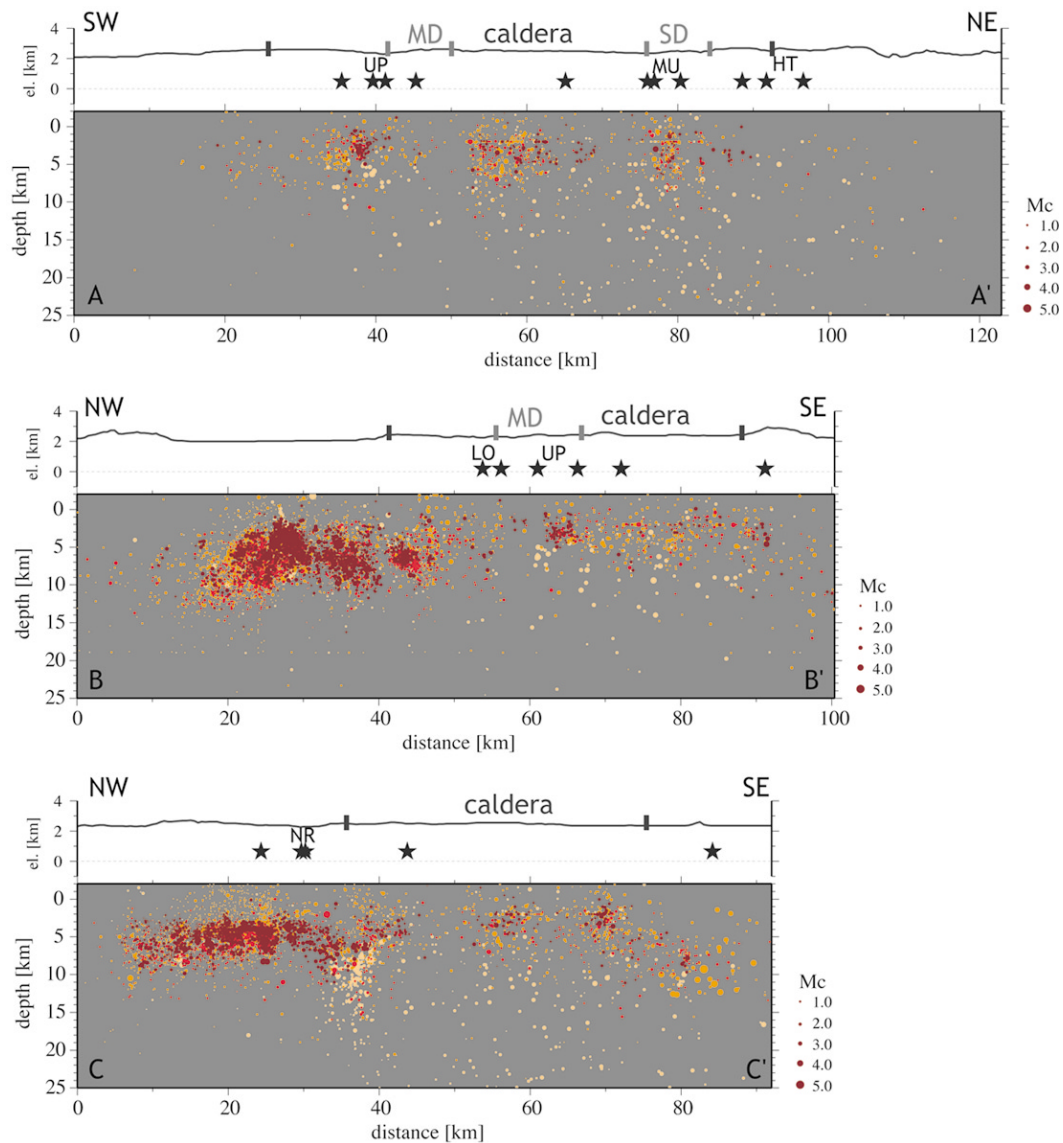
Figure 12. Vertical cross sections of revised earthquake locations along profile AA′ parallel to the long axis of the Yellowstone caldera (top), along profile BB′ across the southwestern caldera (middle), and along profile CC′ across the northeastern caldera (bottom). See Figure 10 for profile locations. Cross sections are 10 km wide. Earthquake locations are color coded by quality and scaled by magnitude. Top of each cross section shows the topography along the profile. Extent of the caldera and resurgent domes are marked by bold black and gray lines, respectively. Stars mark locations of hydrothermal features along the profile. Cross sections are 20 km wide.

their locations unreliable. The nature of these high residuals remains unclear, but we suggest either severe mispicking or timing problems of the data.

The most intense seismicity in the Yellowstone region occurs northwest of the Yellowstone caldera between Hebgen Lake and the northern rim of the caldera. Cumulative seismic moment release in this region is an order of magnitude higher than inside the Yellowstone caldera (Fig. 13). Earthquake locations in the northwestern part form two distinct bands: one stretching in east–west direction from Hebgen Lake to Norris Geyser Basin, the other stretching in a

northwest–southeast direction from Hebgen Lake to the northern rim of the Yellowstone caldera (Fig. 11). The majority of earthquakes in this area occur between 3 and 10 km depth, but focal depths of >12 km are observed close to Hebgen Lake (Fig. 12). The northwestern Yellowstone region is also the locus of several large and intense earthquake swarms, including the 1985 swarm, the largest historic earthquake swarm in Yellowstone (Waite and Smith, 2002). Most of these earthquake swarms appear as individual, large clusters within the band of general seismicity (Fig. 11).

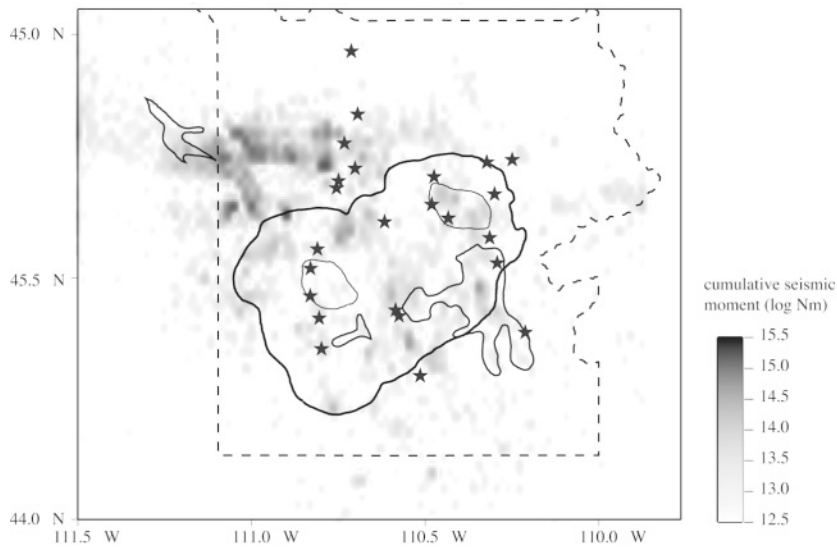Seismicity in the northwestern part of the Yellowstone

Figure 13. Logarithmic cumulative seismic moment release in the Yellowstone National Park region from 1984 to 2002. Local magnitudes were converted into seismic moment using relationships shown in Table 5.

Table 5

Relationships between Local Coda-Magnitude M_c and Seismic Moment M_0 used in This Study (taken from Puskas [2000])

Range	
$M_c \leq 3.08$	$\log M_0 = 1.00 \, M_c + 17.59$
$3.08 \leq M_c \leq 6.0$	$\log M_0 = 1.52 \, M_c + 16.06$

region has been correlated with late Quaternary faults associated with the Hebgen fault system (Smith and Arabasz, 1991; Miller and Smith, 1999). Some of the faults have been mapped (Fig. 11), but some may be buried underneath rhyolitic flows that followed the latest caldera-forming eruption. These faults may have experienced a significant increase in Coulomb failure stress due to the rupture of the 1959 M 7.5 Hebgen Lake earthquake (Chang and Smith, 2002), possibly explaining the intense seismicity in that area. The areas of largest increase in Coulomb failure stress coincide very closely with the two seismicity bands stretching east from Hebgen Lake to Norris Geyser Basin and southeast from Hebgen Lake to the northern rim of the Yellowstone caldera. The modeled increase in Coulomb failure stress decreases east of Norris Geyser Basin and southeast of the northern rim of the caldera (Chang and Smith, 2002). An alternative explanation for the high seismicity in the northwestern part may be postseismic viscoelastic relaxation of the lower crust and upper mantle as a response to the Hebgen Lake earthquake (Chang *et al.*, 2002). Postseismic relaxation will increase stress associated with normal faulting along faults in the Hebgen Lake area, hence encouraging the occurrence of local earthquakes, as evidenced by current GPS data (Puskas *et al.*, 2002) and consistent with the local stress field estimated from local focal mechanisms (Waite and Smith, 2004). The nature of large earthquake swarms in this region, however, remains unclear. A possible explanation might be the migration of fluids released by the crystallization of

magma beneath the Yellowstone caldera, as postulated for the 1985 earthquake swarm that occurred at the transition from uplift to subsidence of the Yellowstone caldera (Waite and Smith, 2002).

Seismicity inside the Yellowstone caldera is diffuse with some individual clusters of earthquakes. The central part of the caldera is apparently aseismic; no seismicity is associated with the Mallard resurgent dome in the western part of the caldera (Fig. 11). Some of the earthquake clusters inside the Yellowstone caldera can be clearly associated with the existence of major hydrothermal areas such as Upper and Lower Geyser Basins, West Thumb Geyser Basin, the central part of the Yellowstone Lake, and the Mud Volcano area (Fig. 11). Intense seismicity is also associated with Norris Geyser Basin close to the northern rim of Yellowstone caldera. Seismicity associated with hydrothermal areas sometimes shows swarmlike behavior clustering in time and space (Upper Geyser Basin and central part of Yellowstone Lake), sometimes seismicity is persistent through time (West Thumb Geyser Basin and Lower Geyser Basin). Cumulative seismic moment release is significant for some hydrothermal areas (e.g., West Thumb Geyser Basin, Mud Volcano area, and central part of the Yellowstone Lake) as compared with the background level (Fig. 13). In general, the focal depths of earthquakes close to hydrothermal areas are shallow (<5 km depth) (Fig. 12). A likely explanation for the seismicity associated with hydrothermal areas is the movement of hydrothermal fluids within the upper shallow crust.

Vertical cross sections reveal a notable shallowing of seismicity across the Yellowstone caldera (Fig. 12). The majority of earthquakes inside the Yellowstone caldera are less than 5 km deep. To the northwest and southeast seismicity deepens remarkably to more than 10 km; the deepest earthquakes (10–15 km depth) are found beneath the Hebgen Lake region. The decrease in focal depths beneath the Yellowstone caldera has been explained by a decrease in depth

of the brittle-ductile transition zone beneath the Yellowstone caldera (Smith and Arabasz, 1991; Miller and Smith, 1999). Elevated temperatures beneath the caldera due to the presence of crystallizing magma will move the depth of brittle-ductile behavior to shallower depth.

Conclusions

We used probabilistic, nonlinear earthquake location to relocate the Yellowstone earthquake catalog. The probabilistic formulation of the problem allows the specific inclusion of *a priori* error estimates through the use of covariance matrices, which makes it superior to traditional, linearized solutions. The probabilistic solution and included error estimates are fully nonlinear and, therefore, can be irregular or multimodal. In irregular or multimodal solutions, traditional error ellipsoids are no longer a correct representation of the true location errors. We used these superior error estimates to classify earthquake locations into four quality classes. The quantification of earthquake locations into four simple quality classes will assist later users to select earthquakes for their purposes. For example, seismotectonic studies will require well located earthquakes that can be found in quality classes A and B.

Our earthquake relocations result in a seismicity pattern that is more focused and shows more detail than the original, routinely obtained earthquake locations. Relocated earthquakes are systematically deeper ($\sim$2 km) than original earthquake locations. We attribute this shift to greater depth to lower than average V_P velocities at shallow depth ($<$5 km) in the northwestern part of Yellowstone, where most of the seismicity occurs. These low V_P velocities are clearly missed by one-dimensional velocity models used to routinely locate earthquakes in Yellowstone.

Yellowstone is driven by volcanic processes embedded in an active extensional tectonic regime of the Basin and Range. The seismicity in Yellowstone contains important information on these processes, but more work is needed to illuminate these. We believe that our new and improved earthquake locations presented in this study will be of fundamental importance for upcoming studies on volcanic and tectonic processes in Yellowstone such as spatial *b*-value mapping or time-dependent seismicity analysis. We will publish our new earthquake locations including the full set of location uncertainties on CD-ROM, which are available on request by contacting the authors.

Although our approach presented in this study is more of a traditional relocation application, probabilistic earthquake location could be used in daily routine work. The combination of probabilistic earthquake location and nonlinear, global search algorithms proves a fast and reliable earthquake location technique given current computing power. A single location of a typical Yellowstone earthquake with eight observations only takes a few seconds to complete. Use of three-dimensional velocity models and probabilistic earthquake location leads to a reliable identification of poorly constrained earthquake locations, which have large location uncertainties that cannot be represented by traditional error ellipsoids. Traditional, linearized earthquake location algorithms such as HYPOINVERSE, which is currently used in Yellowstone, will give unrealistic focal depths for these events, which make up nearly 50% of the Yellowstone earthquake catalog.

References

Benz, H. M., and R. B. Smith (1984). Simultaneous inversion for lateral velocity variations and hypocenters in the Yellowstone region using earthquake and refraction data, *J. Geophys. Res.* **89,** 1208–1220.

Chang, W.-L., and R. B. Smith (2002). Integrated seismic hazard analysis of the Wasatch Front, Utah, *Bull. Seism. Soc. Am.* **92,** 1904–1922.

Chang, W.-L., R. B. Smith, C. M. Meertens, and C. M. Puskas (2002). Rheologic properties of an extending lithopshere from the inversion of postseismic deformation (EDM and GPS) of the 1959 Hebgen Lake, Montana, earthquake, *EOS Trans. AGU* **83,** F635.

Christiansen, R. L. (2001). The Quaternary and Pliocene Yellowstone plateau volcanic field of Wyoming, Idaho, and Montana, *U.S. Geol. Surv. Profess. Pap 729-G*, 145.

Dzurisin, D., K. M. Yamashita, and J. W. Kleinman (1994). Mechanisms of crustal uplift and subsidence at the Yellowstone caldera, Wyoming, *Bull. Volcanol.* **56,** 261–270.

Eberhart-Phillips, D. (1986). Three-dimensional velocity structure in northern California Coast Range from inversion of local earthquake arrival times, *Bull. Seism. Soc. Am.* **76,** 1025–1052.

Eberhart-Phillips, D. (1990). Three-dimensional P and S velocity structure in the Coalinga Region, California, *J. Geophys. Res.* **95,** 15,343–15,363.

Fournier, R. O., and A. M. Pitt (1985). The Yellowstone magmatic-hydrothermal system, U.S.A., in *1985 International Symposium on Geothermal Energy: International Volume*, C. Stone (Editor), Cal Central Press, Sacramento, 319–327.

Hardman, W. L., and R. B. Smith (1991). Earthquake catalog for the Yellowstone National Park region, January 1, 1990 to December 31, 1990, with a contribution by R. A. Hutchinson, Summary of felt earthquakes in Yellowstone National Park, 1990, special report, University of Utah Seismograph Stations, Salt Lake City, Utah, 38.

Haslinger, F., and E. Kissling (2001). Investigating effects of 3-D ray tracing methods in local earthquake tomography, *Phys. Earth Planet. Int.* **123,** 103–114.

Hauksson, E. (2000). Crustal structure and seismicity distribution adjacent to the Pacific and North America plate boundary in southern California, *J. Geophys. Res.* **105,** 13,875–13,903.

Hole, J. A., T. M. Brocher, S. L. Kelmperer, T. Parsons, H. M. Benz, and K. P. Furlong (2000). Three-dimensional seismic velocity structure of the San Francisco Bay area, *J. Geophys. Res.* **105,** 13,859–13,874.

Husen, S., E. Kissling, N. Deichmann, S. Wiemer, D. Giardini, and M. Baer (2003a). Probabilistic earthquake location in complex 3-D velocity models: Application to Switzerland, *J. Geophys. Res.* **108,** doi 10.1029/2002JB001778.

Husen, S., R. B. Smith, and G. P. Waite (2004). Evidence for gas and magmatic sources beneath the Yellowstone volcanic field from seismic tomographic imaging, *J. Volcanol. Geotherm. Res.* **131,** 397–410.

Kissling, E., W. L. Ellsworth, D. Eberhart-Phillips, and U. Kradolfer (1994). Initial reference models in local earthquake tomography, *J. Geophys. Res.* **99,** 19,635–19,646.

Klein, F. W. (1978). Hypocenter location program HYPOINVERSE, *U.S. Geol. Surv. Open-File Rep. 78–694,* 102.

Lee, W. H. K., and J. C. Lahr (1972). HYPO-71 a computer program for determining hypocenter, magnitude and first motion pattern of local earthquakes, Open-File Report, *U.S. Geol. Surv.,* Menlo Park.

Lomax, A., J. Virieux, P. Volant, and C. Thierry-Berge (2000). Probabilistic earthquake location in 3D and layered models, in *Advances in Seismic Event Location,* C. H. Thurber and N. Rabinowitz (Editors), Kluwer Academic Publishers, Dordrecht/Boston/London, 101–134.

Lomax, A., and A. Curtis (2001). Fast, probabilistic earthquake location in 3D models using Oct-Tree Importance sampling. *Geophys. Res. Abstr.,* 3.

Meertens, C. M., R. B. Smith, and C. M. Puskas (2000). Crustal deformation of the Yellowstone caldera from campaign and continuous GPS surveys, 1987–2000, *EOS Trans. AGU* **81,** F1388.

Miller, D. S., and R. B. Smith (1999). P and S velocity structure of the Yellowstone volcanic field from local earthquake and controlled-source tomography, *J. Geophys. Res.* **104,** 15,105–15,121.

Moser, T. J., T. van Eck, and G. Nolet (1992). Hypocenter determination in strongly heterogeneous earth models using the shortest path method, *J. Geophys. Res.* **97,** 6563–6572.

Nagy, W. C., and R. B. Smith (1989a). Earthquake catalog for the Yellowstone National Park region, January 1, 1987 to December 31, 1987, with a contribution by R. A. Hutchinson, Summary of felt earthquakes in Yellowstone National Park, 1987, special report, University of Utah Seismograph Stations, Salt Lake City, Utah, 1–20.

Nagy, W. C., and R. B. Smith (1989b). Earthquake catalog for the Yellowstone National Park region, January 1, 1988 to December 31, 1988, with a contribution by R. A. Hutchinson, Summary of felt earthquakes in Yellowstone National Park, 1988, special report, University of Utah Seismograph Stations, Salt Lake City, Utah, 1–19.

Nava, S. J., and R. B. Smith (1993). Earthquake catalog for the Yellowstone National Park region, January 1, to December 31, 1991, with a contribution by R. A. Hutchinson, Summary of felt earthquakes in Yellowstone National Park, 1991, special publication, University of Utah Seismograph Stations, Salt Lake City, Utah, 1–29.

Nava, S. J., and R. B. Smith (1996). Earthquake catalog for the Yellowstone National Park region, January 1, 1992 to December 31, 1994, with a contribution by R. A. Hutchinson, Summary of felt earthquakes in Yellowstone National Park, 1992–1994, special publication, University of Utah Seismograph Stations, Salt Lake City, Utah, 1–62.

Pechmann, J. C., J. C. Bernier, S. J. Nava, F. M. Terra, and W. J. Arabasz (2001). Correction of systematic time-dependent coda magnitude errors in the Utah and Yellowstone National Park region earthquake catalogs, 1981–2001, *EOS, Trans. AGU* **82,** F809.

Pelton, J. R., and R. B. Smith (1979). Recent crustal uplift in the Yellowstone National Park, *Science* **206,** 1179–1182.

Peyton, S. L., and R. B. Smith (1990). Earthquake catalog for the Yellowstone National Park region, January 1, 1989 to December 31, 1989, with a contribution by R. A. Hutchinson, Summary of felt earthquakes in Yellowstone National Park, 1989, special publication, University of Utah Seismograph Stations, Salt Lake City, Utah, 1–26.

Pitt, A. M. (1987). Catalog of earthquakes in the Yellowstone National Park, Hebgen lake region, Wyoming, Montana, and Idaho, for the years 1973–1981, *U.S. Geol. Surv. Open File Rep. 87–611.*

Puskas, C. M., R. B. Smith, and C. M. Meertens (2002). GPS-derived models of intraplate deformation of the Yellowstone Hotspot, *EOS Trans. AGU* **84,** F1037.

Richins, W. D., R. B. Smith, C. J. Langer, J. E. Zollweg, J. J. King, and J. C. Pechmann (1985). The 1983 Borah Peak, Idaho, earthquake: relationship of aftershocks to the main shock, surface faulting, and regional tectonics, in *U.S. Geological Survey Borah Peak Workshop Redbook, Proceedings of Conference XXVIII,* R. S. Stein and R. C. Bucknnam (Editors), 285–310.

Richter, C. F. (1958). *Elementary Seismology,* W.H. Freeman, San Francisco, 768.

Smith, R. B. (1985). Earthquake data for the Yellowstone National Park region, January 1, 1984 to December 31, 1984, with a contribution by R. A. Hutchinson, Summary of felt earthquakes in Yellowstone National Park, 1984, special report, University of Utah Seismograph Stations, Salt Lake City, Utah, 1–18.

Smith, R. B. (1986). Earthquake data for the Yellowstone National Park region, January 1, 1985 to December 31, 1985, with a contribution by R. A. Hutchinson, Summary of felt earthquakes in Yellowstone National Park, 1985, special report, University of Utah Seismograph Stations, Salt Lake City, Utah, 1–68.

Smith, R. B., and W. J. Arabasz (1991). Seismicity of the Intermountain Seismic Belt, in *Neotectonics of North America,* D. B. Slemmons, E. R. Engdahl, M. L. Zoback, and D. D. Blackwell (Editors), Geological Society of America, Boulder, Colorado, 185–228.

Smith, R. B., and W. C. Nagy (1987). Earthquake catalog for the Yellowstone National Park region, January 1, 1986 to December 31, 1986, with a contribution by R. A. Hutchinson, Summary of felt earthquakes in Yellowstone National Park, 1986, special report, University of Utah Seismograph Stations, Salt Lake City, Utah, 1–24.

Tarantola, A., and B. Valette (1982). Inverse problems = Quest for information, *J. Geophys. Res.* **50,** 159–170.

Thurber, C. H. (1983). Earthquake locations and three-dimensional crustal structure in the Coyote Lake area, central California, *J. Geophys. Res.* **88,** 8226–8236.

Thurber, C. H., and S. R. Atre (1993). Three-dimensional V_P/V_S variations along the Loma Prieta rupture zone, *Bull. Seism. Soc. Am.* **83,** 717–736.

Waite, G. P., and R. B. Smith (2002). Seismic evidence for fluid migration accompanying subsidence of the Yellowstone caldera, *J. Geophys. Res.* **107,** doi 10.1029/2001JB000586.

Waite, G. P., and R. B. Smith (2004). Seismotectonics and stress field of the Yellowstone volcanic plateau from earthquake first-motions and other indicators, *J. Geophys. Res.* **109,** doi 10.1029/2003JB002675.

Wicks, J. R., W. Thatcher, and D. Dzurisin (1998). Migration of fluids beneath Yellowstone caldera inferred from Satellite radar interferometry, *Science* **282,** 458–462.

Department of Geology and Geophysics
University of Utah
Salt Lake City, Utah
  (S.H., R.B.S.)

University of Utah Seismograph Stations
University of Utah
Salt Lake City, Utah
  (R.B.S.)